

## Observation of flow regimes and transitions during a columnar solidification experiment

This content has been downloaded from IOPscience. Please scroll down to see the full text.

2014 Fluid Dyn. Res. 46 041424

(<http://iopscience.iop.org/1873-7005/46/4/041424>)

View [the table of contents for this issue](#), or go to the [journal homepage](#) for more

### Download details:

This content was downloaded by: pubad

IP Address: 89.202.245.164

This content was downloaded on 23/07/2014 at 08:25

Please note that [terms and conditions apply](#).

# Observation of flow regimes and transitions during a columnar solidification experiment

M Stefan-Kharicha, A Kharicha, M Wu and A Ludwig

Montanuniversität Leoben, Department of Metallurgy, Chair for Simulation and Modelling of Metallurgical Processes, Austria

E-mail: [abdellah.kharicha@unileoben.ac.at](mailto:abdellah.kharicha@unileoben.ac.at)

Received 14 November 2013

Accepted for publication 24 April 2014

Published 17 July 2014

Communicated by A D Gilbert and A Gelfgat

## Abstract

Experimental data for the validation of numerical models coupling solidification and hydrodynamics are very rare. Many experiments made in the field of solidifications are performed with pure metals or alloys (Al-Cu, Pb-Sn, etc) which are opaque and do not allow direct observation of the hydrodynamic. Only the results related to solidification such as grain size and orientation, or macro-segregation are usually used for the validation. The present paper is dedicated to the description of well-controlled experiments where both solidification and fluid dynamic can be simultaneously observed. The important point is the almost purely columnar nature of the solidified mushy region. To our knowledge this is the very first reported macro-scale experiment with almost purely columnar solidification where the flow was measured with a PIV technique. The experiments consist in studying the hydrodynamics during the columnar solidification of a H<sub>2</sub>O-NH<sub>4</sub>Cl hypereutectic alloy in a die cast cell. Particle image velocimetry was employed to measure the flow velocity in the liquid bulk. Different flow regimes generated by complex thermo-solutal double diffusive convection were observed. In the beginning of the solidification the solutal buoyancy generates a turbulent flow, which is progressively replaced by the development of stratification from the top of the cell. Later, the stratification leads to the development of a long lasting meandering flow, which filled almost all the liquid region. The kinetic energy of the flow was calculated and it was found out that it decreased with time. The solidification front was smooth and no freckles appeared in the mushy zone. The evolution of the thickness of the mushy zone was measured. As this experiment showed a good reproducibility it represents an excellent benchmark for validation of the numerical models that target the simultaneous prediction of flow dynamics and solidification.

(Some figures may appear in colour only in the online journal)

## 1. Introduction

Solidification is a very complex process. Many parameters can influence the development of the solid, and thus the type of solidification. Columnar, equiaxed or mixed columnar/equiaxed solidification may occur. The cooling rate, the undercooling (temperature below the liquidus temperature without occurrence of solidification), the superheat (melt pouring temperature above liquidus), are important factors, which determine the occurrence of a certain type of solidification. A rapid cooling and a large undercooling will increase the number of nuclei, thus decrease the size of the resulting crystals. The final product will have a fine structure with small grains. Several phenomena take place during solidification: heat and solute transport, diffusion, convection due to temperature or concentration gradient, etc. All of these processes are strongly coupled.

Solutal and thermal buoyancy cause double diffusive convection and the melt flow changes accordingly. The transport of heat and solute can be enhanced by the flow. The quality of the final solid product depends on the type of solidification, which is significantly influenced by the melt dynamic. Double diffusive convection is a very important phenomenon which influences solidification, so its impact on melt flow and solidification will be the focus of this paper.

Lesoult *et al* (1993) conducted some experimental and numerical work to study the influence of natural or forced flow on solidification. It was shown that the melt flow may change the heat transfer conditions, the grain distribution and the segregation. The effect of the melt stirring on the formation of equiaxed zone was definitely established.

During dendritic solidification instabilities in the mushy zone may lead to channel formation. Though those channels lighter interdendritic melt may rise so that a 'chimney'-type plume transports segregated melt into the bulk, where it may effects the motion and solidification of equiaxed crystals. At the end of solidification these channels are filled with descending equiaxed crystals. Such elongated regions of equiaxed crystals in columnar solidified areas are called freckles. They can be as long as the entire casting and represent a severe form of macrosegregation (Flemings 1974). Many ways were tested to suppress the occurrence of freckles: inclination of the mould, rotation, vibration, lid-driven flow, micro-gravity, low temperature gradient.

A large number of experimental and numerical work was dedicated to study casting defects (macrosegregation, A-segregated channels, freckles etc), their occurrence and prevention. On the experimental side different methods, such as shadowgraphy, computer tomography (CT), die injection, and particle image velocimetry (PIV) were used for visualisation of the phenomena which happens during solidification.

Chen and Chen (1991) presented an overview on channel and freckle formation concentrating on directional solidification of ammonium chloride. They studied the occurrence of plumes in the fluid region just above the mushy zone when the temperature gradient is large. They estimated the porosity across the mushy zone (using CT), the solute Rayleigh number, the inner diameter of the channel, the average size of the dendrites and the average flow velocity deep down in the mushy zone.

Channel formation and their prevention were already studied in the 1980s by Sample and Hellowell (1982, 1984) and so, implicitly the double diffusive convection during the solidification. They tried to understand the mechanism of formation and propagation of channels,

using a stationary mould, vertical, or inclined (between 20 and 30 deg.) or rotating at <5 rpm up to 10 rpm.

By means of shadowgraph and die techniques Magirl and Incropera (1992) studied unidirectional solidification and solidification from both sides and the bottom. In the last case, equiaxed grains formed (as consequence of columnar dendrites fragmentation), and enhanced the motion in the double diffusive convection cells, which impeded the motion of plumes.

A more recent work to understand double-diffusive convection during solidification in hypereutectic  $\text{NH}_4\text{Cl-H}_2\text{O}$  alloys was done by Shih and Tu (2009). By means of PIV they measured flow fields and for two concentrations (25 wt.% and 28 wt.%) they reported several flow circulation rolls near the mushy zone and in the melt. Shih *et al* (2013) experimented with lid-driven flow in order to suppress freckles. They also measured the temperature and the concentration during solidification and observed that reducing the temperature and concentration gradient reduced the number of freckles. The experimental results showed that increasing the slider speed suppressed the development of double-diffusive convection effectively.

Tan (2005) tried mechanical vibration of the test cell to eliminate freckle formation. He varied initial concentration, temperature of the base plate and inclination. Experiments showed that for all hypereutectic alloys channels formed. The concentration increase will diminish the number of channels but will make them more pronounced. Decreasing the temperature of the base plate will decrease the number of channels. Also the amplitude and frequency of vibrations influence the formation of channels.

Saffie *et al* (2013) observed what they called ‘snowing’ phenomenon in a couple of experimental studies. Some were performed with unidirectional solidification, where equiaxed crystals formed near the bottom and were then carried up by thermo-convective flows and finally fell down similar to real snow in winter. The results showed that increasing the solute concentration will decrease the onset of ‘snowing’, but increase the size of equiaxed crystals. Varying the temperature does not affect the onset of ‘snowing’ but lengthens the period of the phenomenon.

Neilson and Incropera (1991, 1993) and Christenson *et al* (1989) worked on the unidirectional solidification of transparent binary  $\text{NH}_4\text{Cl-H}_2\text{O}$  alloys. Experiments and simulations of the impact of induced and rotated fluid motion on the development of the channel formation were performed. It was established that freckles originate from flow channels that nucleate in the mush. Another significant factor that influences channel formation turned out to be the mushy zone permeability. Their experimental study showed that radially induced flow by rotation and tilting of the mould could inhibit channel formation.

Aggregations and channel formation (Solomon *et al* 1999) during the solidification of ammonium chloride were investigated in a thin Hele-Shaw cell, with the cell being heated from below and cooled from above or vice versa. In the former case a lot of equiaxed crystals occurred and deposited so that aggregations formed. In the second case when the cell is cooled from below and heated from above no deposition of crystals was observed and a compact mushy zone formed. Somehow, if the environment was cool comparing to the liquidus temperature of the solution, some ballistic deposition occurred and the mushy layer, which formed now as mixture of dendrites and ballistic deposition, was found to be more permeable. In this case the formation of channels and plumes was enhanced. The ballistic deposition was also increased in the case when the cell was tilted. However, artificially induced flow in the liquid and in the mushy layer did not enhance the channel formation. These experimental data were supported with some numerical simulations which showed the same phenomena.

Chen (1997) performed experimental and numerical work on the double-diffusive layer during the directional solidification of a 28 wt%  $\text{NH}_4\text{Cl}$ -water, and measured the position of the melt/mush interface, the height of the eutectic solid, the number of plumes, the height of convective fingers and the position of each interface between the double diffusive layers. The growth of the mush was manipulated by the temperature of the bottom plate  $T_B$ . It was shown that the time to reach the maximum plumes number depends on the value of  $T_B$ ; the time is shorter for lower  $T_B$ . The time for an onset of double-diffusive layering was also found to be shorter for lower  $T_B$  because double-diffusive layering occurred when the maximum number of plumes has established. However, the thickness of the layers did not depend on the  $T_B$ .

Beckermann and Viskanta (1988, 1989) studied numerically and experimentally the double-diffusive convection occurring during solidification. Remelting of columnar dendrites was found to be a possible condition for channel formation.

Experimental data performed by Stefan-Kharicha *et al* (2009) was used in a first attempt to model the columnar growth of ammonium chloride alloy in a die-cast cell (Könözy *et al* 2009). A direct comparison of the distribution of the columnar growth at the end of their solidification experiment showed a qualitatively good agreement between experimental and numerical results.

Kharicha *et al* (2012) developed a cellular automaton 2D model to study double-diffusive convection during binary alloy solidification. Different flow regimes were reported and the existence of a turbulent regime was related to the generation of individual plumes at each columnar dendrite.

Ahmadein *et al* (2014) employed a 5-phase model (Wu *et al* 2010a, 2010b) to simulate the experimental data presented here. The 5 phases in the model represented the solid equiaxed crystal, the solid columnar dendrite, the extradendritic liquid melt, the intradendritic melt inside the equiaxed crystal and the intradendritic melt inside the columnar mushy zone. Different flow patterns were observed and the evolution of the solid front was calculated. Qualitative results were obtained but more efforts should be put for further quantitative comparison.

Experiments reporting both the flow hydrodynamics and the solidification are very scarce. In the present paper experiments with the transparent alloy  $\text{NH}_4\text{Cl}$ - $\text{H}_2\text{O}$  and almost pure columnar solidification, where the mushy zone grows with a macroscopic flat envelope, are presented. The geometry and the experimental conditions are similar to the experiments previously performed by Kharicha *et al* (2013a, 2013b). Here, we report only the experimental data where no freckles developed and where equiaxed crystals were rare. However, we have to admit that for us the reasons why sometimes freckles and equiaxed crystals appear and sometimes not are still unclear. Nevertheless, we postulate the existence of a kind of bifurcation where a small smooth change of a parameter might induce a totally different behaviour of the hydrodynamic-solidification system. It is known that the equiaxed crystals are formed by (a) nucleation, (b) fragmentation of secondary arms by re-melting or (c) fragmentation of secondary arms by mechanical breaking. All three mechanisms may be effected by hydrodynamics.

The reproduction of experiments with heavy equiaxed crystal falling represents still a challenge for numerical simulations. Correlations for the momentum transfer between the liquid phase and the falling crystals are only known for the limit of very diluted equiaxed fraction. For larger volume fractions the effective viscosity and the drag coefficients are unknown. In comparison the permeability of static columnar dendrites are much better known. This is why an experiment with almost pure columnar dendrites constitutes an excellent data set for the validation of numerical simulations. From the experiments presented

in this paper we have extracted the following parameters: thickness and growth of the mushy zone, flow behaviour (in terms of flow regimes) and kinetic flow energy (KE).

## 2. Experimental setup

The transparent 29.57 wt.% ammonium chloride-water alloy was chosen for the solidification experiments. The Particle Image Velocimetry (PIV) set-up consists of a source light (in our case a Nd-YAG double pulsed laser) and two CCD cameras. First CCD camera was used to record the flow movement and the second to record the equiaxed crystals movement. To measure the velocity of the flow a tracer particle is needed. To distinguish between the flow and the crystals movement a special tracer particle (polyamide particle coloured with Rhodamine B) was used. Each CCD camera was equipped with a specific filter. For the CCD camera which recorded the flow movement, an orange filter of 570 nm and for the second CCD camera, which was employed to measure equiaxed crystals velocities, a green filter of 532 nm were used. The commercial software, FlowManager<sup>1</sup>, was used for recording and analysing of the images.

The dimensions of the test cell (Kharicha *et al* 2013a, 2013b) were 10\*10\*1 cm<sup>3</sup>. It's laterals and bottom walls were made of brass. The front and back walls were made of commercial transparent glass. The top of the cell was left open. The temperature of the brass walls was controlled via a circulation bath by applying a linear cooling rate of 1.2 K min<sup>-1</sup>. The room temperature for the experiments was maintained between 19 °C and 21 °C. The position of the test cell was horizontally adjusted.

The experimental procedure followed always the same steps. First the alloy was prepared. The necessary amount of NH<sub>4</sub>Cl powder was weighted and mixed with distilled water. The mixture was heated up until the powder was completely dissolved. The solution was then poured into the test cell, which was previously heated to the same temperature. The height of the liquid in the cell was set to 8 cm. The system (test cell with solution) was left untouched for 30 min with keeping cell walls at the initial pouring temperature. In this way a quasi steady-state situation, avoiding the residual hydrodynamic turbulence, was achieved before the solidification experiment started. The time when the cooling bath was switched to the predefined cooling temperature of 5 °C is the starting point of our experiment,  $t_0$ . In all our experiments we have measured a constant cooling rate in the brass walls until the bath reached around 5 °C (Kharicha *et al* 2013a). Due to the meander-shaped cooling channel in the brass parts and the high flow rate of the cooling water we measured a uniform temperature in the brass walls. Note that with 29.57 wt.% NH<sub>4</sub>Cl as solute, the NH<sub>4</sub>Cl-H<sub>2</sub>O solution will not completely solidify when being cold down to 5 °C. According to the phase diagram the remaining liquid may have reduced its NH<sub>4</sub>Cl content to around 24 wt.%. That's a difference of  $\Delta C = 6$  wt.%.

According to the NH<sub>4</sub>Cl-H<sub>2</sub>O phase diagram the liquidus temperature for a 29.57 wt.% NH<sub>4</sub>Cl alloy is 37 °C. We decided to make several experiments with different starting temperatures: 5 °C, 10 °C, 15 °C and 20 °C above liquidus. For each superheat we performed two experiments with identical experimental conditions. The superheat is known to control the type of solidification: equiaxed or columnar. If ahead of the columnar front an undercooled liquid and a sufficient large number of equiaxed exist then columnar dendrites will be stopped by the equiaxed crystals and a so-called Columnar-to-Equiaxed Transition, CET, occurs. For the purpose of this paper the authors have chosen only experiments which revealed an

<sup>1</sup> FlowManager is a trademarked software from Dantec Dynamics, DK (<http://www.dantecdynamics.com/>).

extremely small number of equiaxed crystals during almost pure columnar growth. None of the experiments in this paper showed the presence of any channels, chimneys, or plumes during the whole solidification process.

### 3. Results and discussion

#### 3.1. Flow visualisation and regimes

The cooling from the walls and the occurrence of solidification generate various and complex phenomena. Regardless of the superheat which was employed, each experiment followed similar flow regimes as described in the previous analysis of Kharicha *et al* (Kharicha *et al* 2013a, 2013b), where however massive equiaxed crystals were present. Only the time when a regime changes into the next depends on the superheat. In this section, the experiment with 5 °C superheat will be described first. The other experiments with different superheats (10 °C, 15 °C and 20 °C) will be detailed in section 3.2. In table 1 the values related to the onset time of the different flow regimes are gathered for the different experiments.

**3.1.1. Thermal symmetrical regime (TH).** Before starting the cooling, the solution was untouched for 30 min and a stable flow pattern with ascending flow along the vertical walls and a descending flow in the centre established (not shown). When the cooling bath was switched on this stable flow pattern was disturbed. However, after a few minutes two symmetrical rolls with descending flow along the vertical walls and ascending flow in the centre caused by thermal buoyancy appeared (figure 1). This laminar stable flow constituted the first regime which we call TH regime (thermal symmetrical). The time to reach this stable flow regime was, for the case of 5 °C superheat, around 7 min and it lasted for around 7 min.

When the cell walls reached the necessary undercooling for heterogeneous nucleation, dendritic crystals appeared at the brass walls. They grew first in form of very small islands, which developed and finally covered the whole wall surface (side and bottom wall simultaneously) with a very fine layer of dendritic crystals. In the case of the 5 °C superheat, solidification occurred around 12 min after the cooling was started. Although visible solidification at the cell walls happened the flow pattern stayed almost unchanged for 1–2 min.

**3.1.2. Perturbed thermal regime (PTH).** At around 13–14 min, perturbation of the symmetrical flow appeared by small eddies around the fine solid layer which formed at the side walls. These small perturbation of the flow pattern concerned only the vicinity of the solid, the bulk flow kept the same symmetrical convection rolls (figure 2). We call this regime PTH (perturbed thermal). It is the shortest regime as it lasted only around 2 min.

**3.1.3. Turbulent regime (TU).** Then, 16 min after starting cooling, small plumes started to rise from the bottom mush. They are originated by the rejection of lighter solute during solidification of the mushy zone and thus transport solute enriched melt into the bulk. So solutal buoyancy started to play an important role on the development of the flow. Now, the symmetry of the flow pattern became completely destroyed (figure 3). This regime we call TU as it is turbulent as we will show later. The TU regime lasted approximately 8 min. The simulation work of Kharicha *et al* (2012) suggested that the above mentioned solutal plumes are the origin of the TU regime. As shown later (figures 7 and 10), the strongest solidification rate occur during the TU regime, where strong interaction between plumes and perhaps inverse cascade of eddies takes place (Bizon *et al* 1997).

**Table 1.** Points in time when the different flow regimes occurred during the solidification process for different superheats between 5 °C and 20 °C.

Experiment	Initial temp. (Superheat)	Room temp.	TH Thermal stable regime	Time for first solidification	PTH Perturbed thermal regime	TU Turbulent regime	Occurring of equiaxed crystals	TU—ST Turbulent-stratified regime	MF Meandering flow regime
A	42 °C (+5 °C)	21 °C	7 min.	12 min.	14 min.	16 min.	22 min.	24 min.	32 min.
B	42 °C (+5 °C)	20 °C	7 min.	12 min.	13 min.	15 min.	22 to 29 min.	23 min.	32 min.
C	47 °C (+10 °C)	20 °C	7 min.	15 min.	17 min.	18 min.	23 to 32 min.	24 min.	34 min.
D	47 °C (+10 °C)	20 °C	9 min.	15 min.	17 min.	18 min.	24 to 32 min.	25 min.	37 min.
E	52 °C (+15 °C)	19 °C	7 min.	16 min.	18 min.	19 min.	23 to 33 min.	29 min.	38 min.
F	52 °C (+15 °C)	20 °C	7 min.	18 min.	19 min.	21 min.	25 to 34 min.	27 min.	36 min.
G	57 °C (+20 °C)	20 °C	7 min.	20 min.	21 min.	23 min.	24 to 37 min.	32 min.	36 min.
H	57 °C (+20 °C)	19 °C	8 min.	19 min.	20 min.	23 min.	26 to 37 min.	30 min.	36 min.

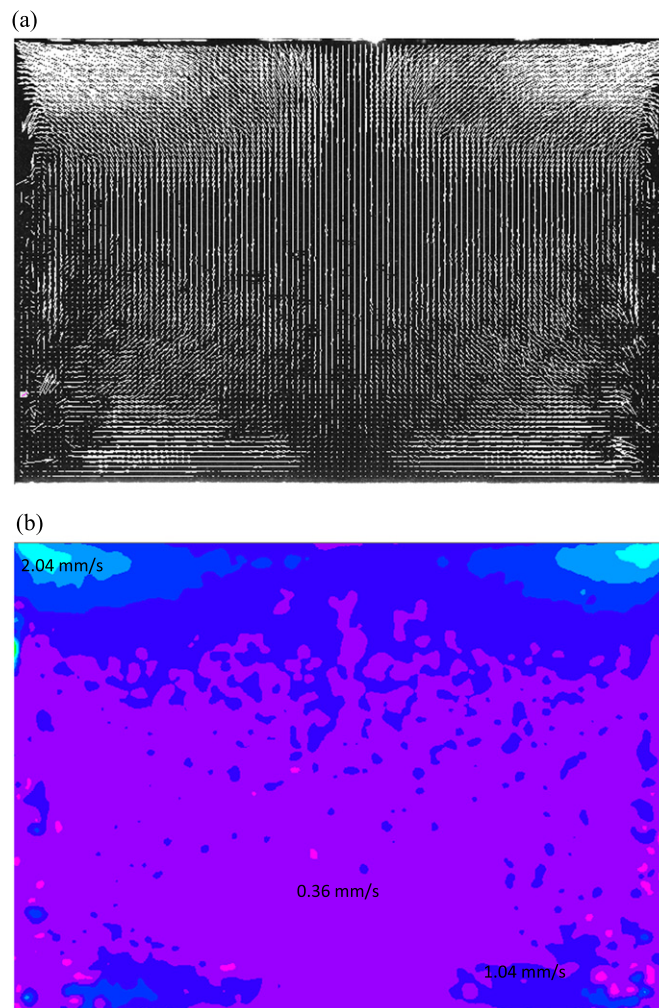


**Figure 1.** Thermal symmetric (TH) flow regime during the solidification of 29.57 wt.%  $\text{NH}_4\text{Cl}$  alloy for an initial superheat of  $5^\circ\text{C}$ . (a) Measured flow field at  $t = 10$  min and (b) measured velocity magnitude of the flow at  $t = 10$  min.;  $v_{\min}$ (purple) =  $0.36 \text{ mm s}^{-1}$ ;  $v_{\max}$ (turquoise) =  $2.04 \text{ mm s}^{-1}$ .

The occurrence of turbulence can be estimated by considering the thermal and the solutal Rayleigh number. For a vertical wall the critical Rayleigh number for the occurrence of turbulence is  $Ra = 10^9$  (Bejan 1993). Previous analysis performed by Kharicha *et al* 2013b has shown that the thermal Rayleigh number is too small ( $\sim 10^8$ ) to induce a transition from lamellar to turbulence. The solutal Rayleigh number can be estimated by considering the difference between the initial and final  $\text{NH}_4\text{Cl}$ -concentration given by the phase diagram. Using known material properties, Kharicha *et al* 2013a showed that  $Ra = 2.2 \cdot 10^9 \cdot \Delta C$  ( $\Delta C$  in wt.%) yields for  $\text{NH}_4\text{Cl}$  as solute in  $\text{H}_2\text{O}$ . As stated above we have a difference between the initial and the final solute content of  $\Delta C = 6$  wt.%, which would lead to  $Ra = 1.32 \cdot 10^{10}$ , so far greater than the critic Rayleigh number. Thus, the onset of turbulence can easily be reached since a concentration difference of only  $\Delta C = 4.5$  wt.% is enough to obtain  $10^9$ . When

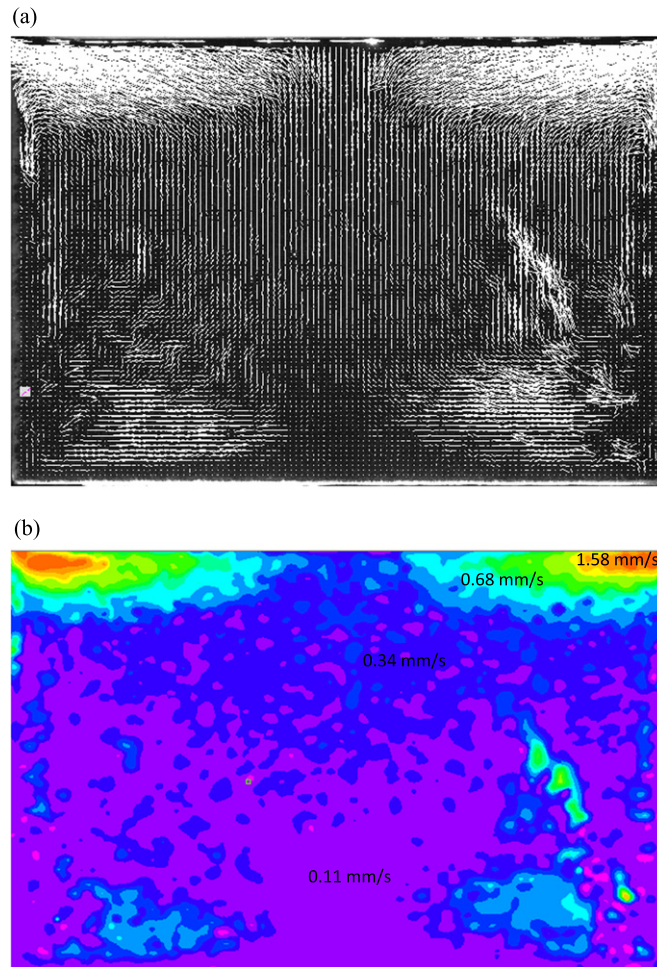


**Figure 2.** Perturbed thermal flow regime (PTH) during the solidification of 29.57 wt.%  $\text{NH}_4\text{Cl}$  alloy for an initial superheat of  $5^\circ\text{C}$ . (a) Measured flow field at  $t = 13$  min and (b) measured velocity magnitude of the flow at  $t = 13$  min.;  $v_{\min}$ (purple) =  $0.11 \text{ mm s}^{-1}$ ;  $v_{\max}$ (orange) =  $1.58 \text{ s}^{-1}$ .

the turbulent regime is effectively observed the solutal Rayleigh number exceeds probably  $10^{10}$ .

However the situation is more complex since thermal buoyancy and inertia effects are simultaneously acting, whereby, thermal is acting in the opposite direction as solutal buoyancy. When a parcel of liquid cools at the vicinity of a wall its density increase because of the thermal buoyancy but decreases because of solidification (rejected solute contains more water and so it is lighter). This is why despite the high magnitude of the solutal Rayleigh number, most of the flow regimes observed could be qualified as laminar with (i) very large and coherent structures, and (ii) quasi divergence free 2D velocity fields. In opposite, the ‘turbulent’ regime shows the existence of a 3D highly transient and incoherent eddies of different scales.

The presence of the columnar mushy region can also explain the low level of turbulence observed. A flow convection exist also within this porous media, but it is not measurable

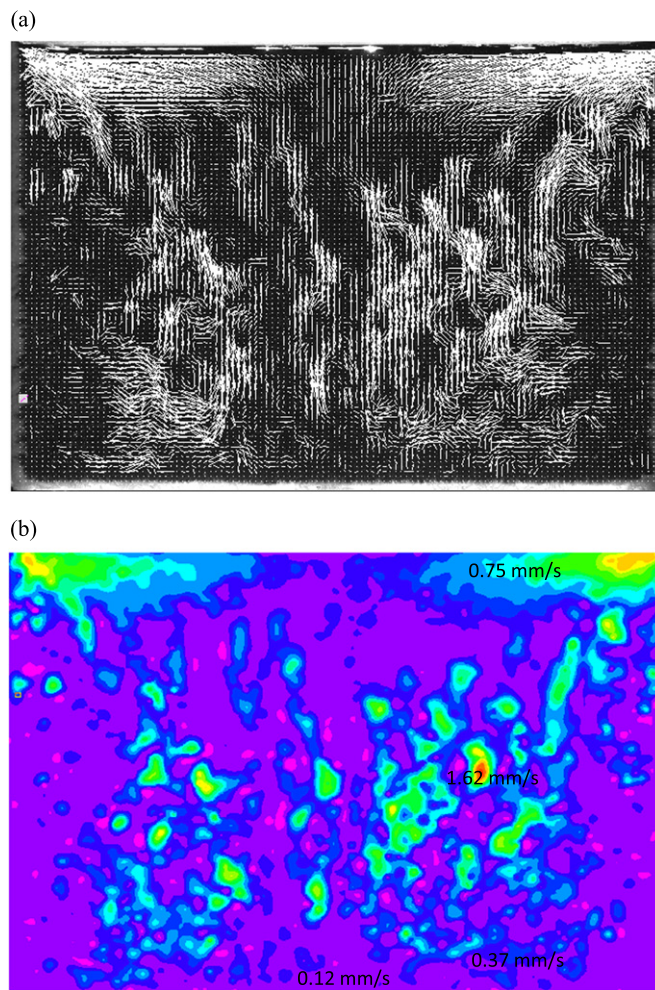


**Figure 3.** Turbulent flow regime (TU) during the solidification of 29.57 wt.%  $\text{NH}_4\text{Cl}$  alloy for an initial superheat of  $5^\circ\text{C}$ . (a) measured flow field at  $t = 15$  min and (b) measured velocity magnitude of the flow at  $t = 15$  min.  $v_{\min}$ (purple) =  $0.12 \text{ mm s}^{-1}$ ;  $v_{\max}$ (orange) =  $1.62 \text{ mm s}^{-1}$ .

experimentally with the present PIV method. By damping the turbulence (high Rayleigh number), the mushy region contribute probably to the ‘laminarization’ of the flow in this experiment.

**3.1.4. Turbulent—stratified flow regime (TU-ST).** At about 23–24 min after start cooling, the eddies present in the bulk had still a turbulent nature (figure 4). At the top of the cell the start of a flow stratification could be observed; already two symmetric layers are visible. This lasted for about 6 min for the case with  $5^\circ\text{C}$  superheat. This regime was labelled the TU-ST (turbulent-stratified). In previous publication of the authors (Kharicha *et al* 2013a, 2013b) a coherent chaotic regime developed at this point in time; the eddies became large and coherent. Now, the lack of equiaxed crystals in the bulk may be at the origin of the missed coherent chaotic regime.

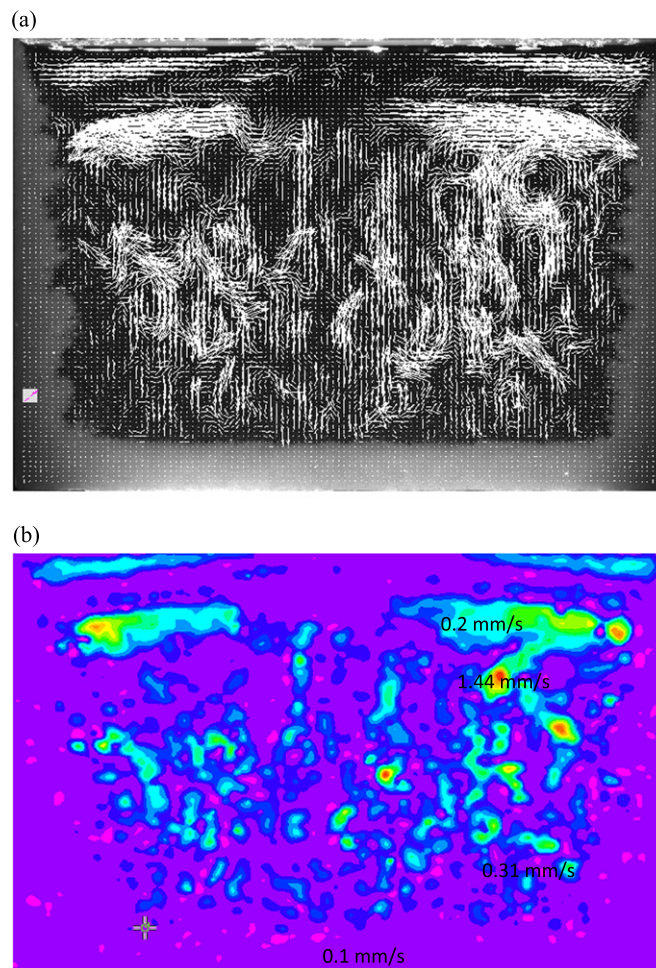


**Figure 4.** Turbulent stratified flow regime (TU-ST) during the solidification of 29.57 wt.%  $\text{NH}_4\text{Cl}$  alloy for an initial superheat of  $5^\circ\text{C}$ . (a) Measured flow field at  $t=23$  min and (b) measured velocity magnitude of the flow at  $t=23$  min.;  $v_{\min}(\text{purple})=0.1 \text{ mm s}^{-1}$ ;  $v_{\max}(\text{orange})=1.44 \text{ mm s}^{-1}$ .

Until 22 min after start cooling, solidification occurred only in a columnar form. The growth was very uniform and smooth along the whole length of the walls. No channels formed in the mushy zone, nor chimneys with the release of equiaxed crystals, as in previous publications (Kharicha 2013a, 2013b). However, at 22 min some equiaxed grains formed very close to the lateral walls. Mainly those grains flowed down, along the borders of the lateral solid front, until they reached the bottom, but some were captured in the lateral columnar zone and continue to grow. This rain of equiaxed crystals lasted 9 min, mainly during the turbulent-stratified flow regime.

**3.1.5. Meandering flow regime (MF).** After around 32 min the stratification of the flow, from the top to the bottom, became clearly visible (figure 5). The melt flow was organized horizontally in several layers from one side to the other side of the lateral columnar mushy zone. The protrusion of the vertical mushy front topography in interaction with the thermo-solutal convection may result in such a meandering flow. Approaching the bottom mushy

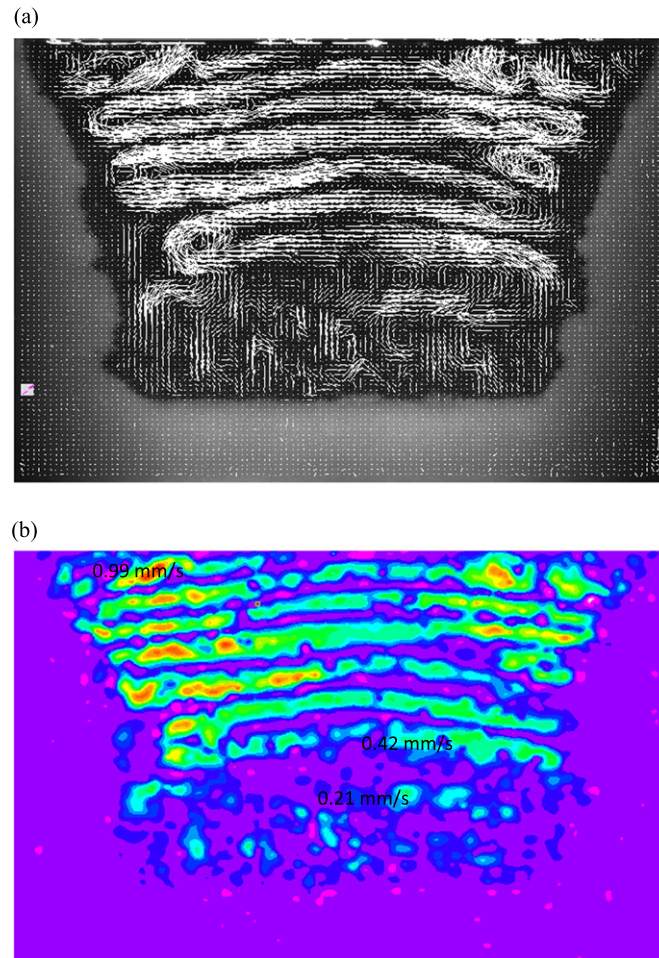


**Figure 5.** Meandering flow regime (MF) during the solidification of 29.57 wt.% NH<sub>4</sub>Cl alloy for an initial superheat of 5 °C. (a) Measured flow field at  $t = 32$  min and (b) measured velocity magnitude of the flow at  $t = 32$  min.;  $v_{\min}$  (dark blue) = 0.21 mm s<sup>-1</sup>;  $v_{\max}$  (orange) = 0.99 mm s<sup>-1</sup>.

front the melt flows into the mushy zone at some locations and flows out of the mush at other locations. This stage is called the Meandering Flow regime (MF) and is the longest of all flow regimes. It lasted more than 20 min. The mechanism at the origin of this snaky flow is still unclear. When no visible growth of the columnar mushy zone took place, the solidification experiment was considered as finished. This happened about 50 min after start cooling.

### 3.2. Reproducibility of experiments with different superheats

Four sets, two experiments each, with 5 °C up to 20 °C superheats were performed. It turned out that the solidification regimes were similar, only the points in time when these regimes appeared were different. In table 1 the corresponding data are gathered.

Analysing the data in table 1 it become obvious that the first flow regime TH is not influenced by the superheat employed. Regardless the amount of superheat it always took

around 7 min to reach the corresponding natural convective flow pattern. Regime TH lasts always 1–2 min after first solidification occurs. The beginning of solidification is very important for the evolution of the flow pattern, as it initializes solutal buoyancy and with that double-diffusive convection. Visible solidification first appeared along the walls 15 to 20 min after the cooling was switched on. The exact point in time at which visible solidification occurred depends clearly on the initial temperature. The larger the superheat the longer it takes to reach the necessary undercooling for heterogeneous nucleation.

As reported above the PTH regime described the transition between the TH and the TU regime. Independent of superheat it lasted only 1–2 min.

Between 18 to 23 min, due to the thermo-solutal buoyancy, plumes developed in the bulk liquid. Large variations in flow velocities magnitude could be observed in the melt. This is characteristic for the turbulent flow regime.

Between 23 to 26 min a new phenomenon occurred, equiaxed crystals started to appear along the lateral mushy zone which developed on the side walls. For all experiments presented in this paper, the equiaxed crystals concentrated only next to the lateral mush, phenomenon which we call ‘rain crystals’. The rain crystals occurred only between 8 and 13 min. It could be observed that for the smallest superheat the length of this phenomenon was the shortest (7 min), and for the highest superheat the rain crystals lasted the longest time (13 min).

A few minutes after the onset of the rain crystals, stratification began in the TU regime. At the top of the cell the flow started to stratify and two symmetrical layers developed (TU-ST). The flow stratification continued until the MF regime, when it was covering the whole cell from top to bottom.

In the meander flow regime (MF), the solutal buoyancy and the thermal buoyancy (the two main forces) equilibrated and gave an organized structure to the flow. The flow organized horizontally in 4 to 7 parallel layers. This flow stratification occurred 32 min after cooling was started, but was perfect at 36 to 38 min. Not only the time when solidification started was different for the different superheats, but also the wall temperature at which the first crystals were visible along the walls. For lower superheat of 5 °C and 10 °C this wall temperature was around 28 °C, for the medium superheat of 15 °C we got 29.3 °C and 28 °C, and for the largest superheat of 20 °C we got 31 °C. Obviously, the larger the superheat employed, the higher the wall temperature when first crystals occur at the wall.

### 3.3. Start of a new flow regime

Accounting for the start of a new flow regime was difficult, because in many cases a transition stage between regimes existed. Once solidification has started the flow behaviour changed clearly, but to distinguish between PTH and TU regimes is very difficult. In fact, the PTH can be considered only as a transition between TH and TU, when turbulence is observed only locally. For this reason the onset of the TU regime can be considered 1 or 2 min before the given time in the table 1.

### 3.4. Total kinetic flow energy

The kinetic energy was calculated for each experiment from the beginning of cooling till no further solid formed (approximately 40 min). Of course, only the total kinetic energy contained in the visible liquid was considered, as the portion present within the mushy region remained invisible. The total flow kinetic energy was calculated with the following equation

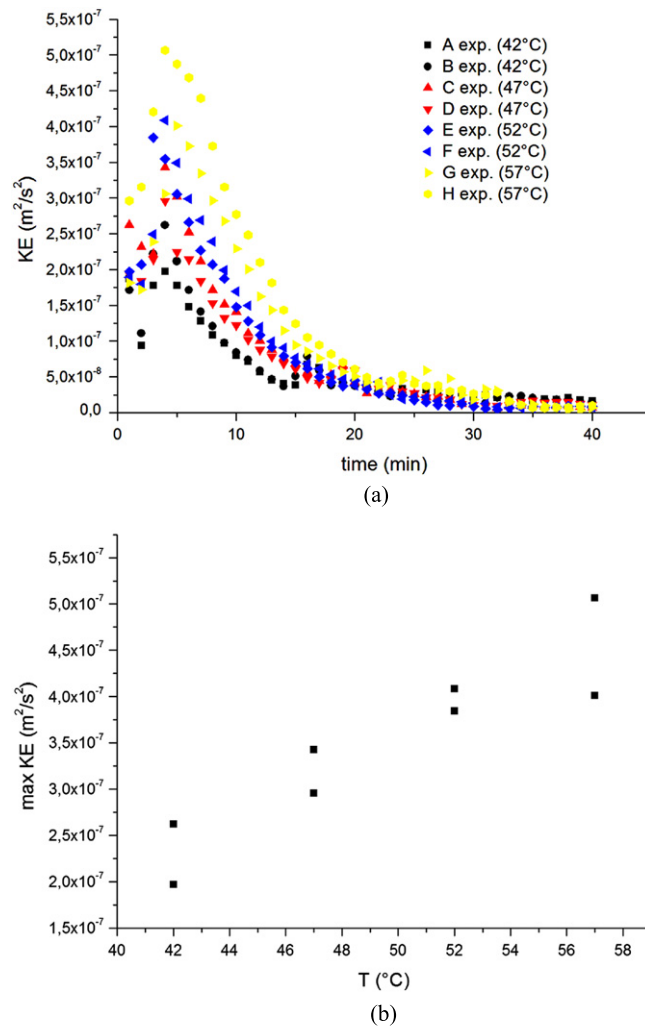


**Figure 6.** (a) General evolution of the flow kinetic energy during solidification for different superheats; (b) linear variation of the maximum flow kinetic energy with superheat.

$$KE = \rho * S * \varepsilon * \sum_{i=1}^N \frac{1}{2} U_i^2 / N \quad (1)$$

where  $N$  is the total number of velocity vectors obtained by the PIV measurement.  $\rho$  is the density of the liquid,  $S$  the total vertical surface of the liquid in the cell at the beginning of the experiment and  $\varepsilon$  the thickness of the cell. Although there is a change in density with temperature and concentration, the difference doesn't exceed 1% between the beginning and the end of the experiment. Therefore the density is considered as constant.

As shown in figure 6(a), the flow kinetic energy decreases continuously with time except for a short time during the turbulent regime.

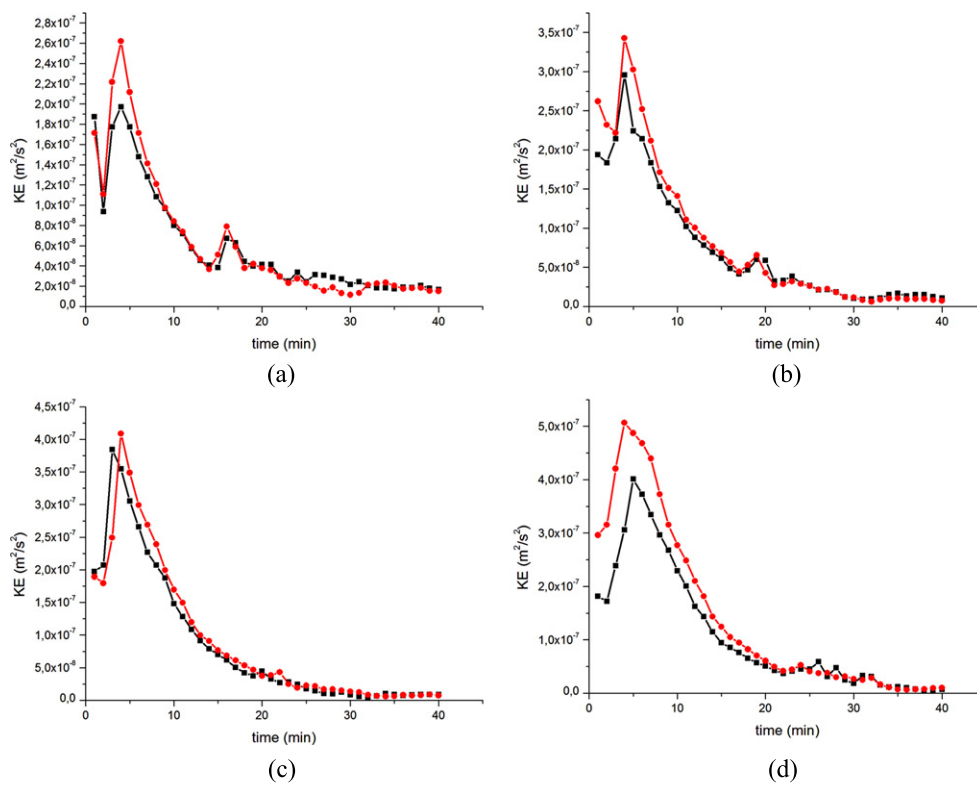


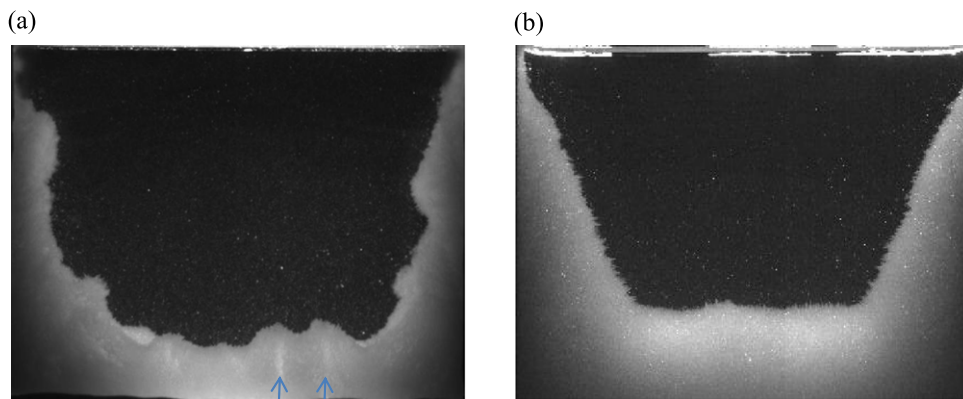
**Figure 7.** Evolution of the flow KE during solidification for different starting temperatures: (a) 42 °C (experiments A and B); (b) 47 °C (experiments C and D); (c) 52 °C (experiments E and F); (d) 57 °C (experiments G and H).

### 3.5. Reproducibility of experiments in terms of kinetic energy (KE)

The flow kinetic energy evolution follows the same decreasing tendency for all experiments regardless the superheat (figure 6(a)). The maximum value is reached 3 to 5 min after the start of the cooling bath. In this short period the flow kinetic energy follows a down-up fluctuation. From this point the flow kinetic energy continues to decrease exponentially. Until around 20 min the decrease is very strong, between 20 and 30 min the decrease is extremely slow but weak variations can appear, and after 30 min it is almost constant. A small elevation of the flow kinetic energy was always observed during the TU regime.

It can be seen in figure 6(a) that even though the global tendency is the same, some differences exist. At the beginning of the cooling, along the lateral walls a strong downwards flow occurs. The boundary layer of this downwards flow is very thin. Even though clearly visible with the naked eye, the software (Flow Manager) cannot resolve it correctly. For this reason the flow kinetic energy at the beginning of the experiment presents some differences (the error can be large), sometimes between experiments with the same superheat.

Straightforward is that the larger the superheat, the larger is the maximum values for the flow kinetic energy. In figure 6(b) it can be seen that the maximum value for the flow kinetic energy varies linearly with the starting temperature.



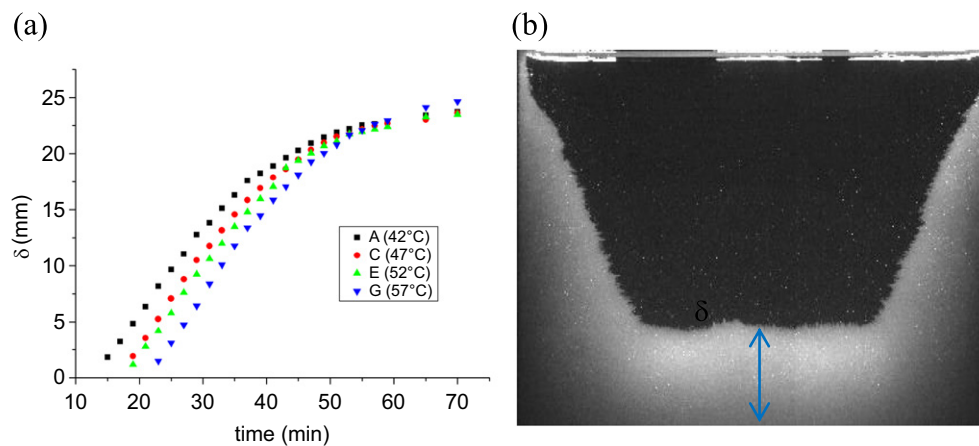
**Figure 8.** Comparison of mushy zone shape. (a) Solidification process which is dominated by equiaxed crystals. Note the freckle formation in the mush, taken from (Kharicha, 2013). (b) Solidification process where the presence of equiaxed crystals can be neglected and practically pure columnar solidification happens.

Figure 7 shows the flow kinetic energy for different experiments with different superheats. Each experiment was done two times. It can be observed that the reproducibility is very good. In figures 7(b) and (d) small differences can be seen at the starting point for the two experiments. This is due to the fact that the upwards flow along the lateral walls at the very beginning of the cooling is very difficult to catch, as the boundary layers are extremely thin. After a very short decrease ( $\sim 3$  min) the flow kinetic energy increases shortly (2–3 min) until it reaches the maximum value. Then the flow kinetic energy decreases continuously. With a larger starting temperature the TH regime becomes longer, as the TH regime lasts as long as no solidification occurs and this depends on the applied superheat (section 3.2). Even though the global evolution of the flow kinetic energy decreases, very weak variations subsist and these small peaks are related to the onset of the TU regime (figure 7). As previously explained the start of the TU regime is very difficult to determine. For this reason, it seems that the TU starts one minute after the peak in figure 7(a), directly at the maximum peak value in figure 7(b) and before the peak in figures 7(c) and (d). Also one might think that the superheat has an influence on the TU-ST regime, as it is shorter for 15 °C and 20 °C superheat compared to 5 °C and 10 °C superheat. These are vague observations which depend on the subjective assessment of the different regimes.

### 3.6. Solidification rate and columnar thickness

During our columnar solidification experiments, where dendrites grew from all walls, sides and bottom, the mushy zone thickness along the bottom wall was very uniform and the boundary between the mushy zone and the liquid appeared smooth (figure 8(b)). However, sometimes quite a severe amount of equiaxed crystal occur, which can stick to the mould wall, grow together with the columnar front or settle down and form a sediment of crystals. Figure 8 shows the mushy zone for an experiment where a huge amount of equiaxed crystals were present (a) and for an experiment where practically the amount of equiaxed can be neglected (b).

In case of practically pure columnar solidification, the advance of the boundary between the mushy zone and the bulk liquid can be accurately measured. In figure 9(a) the measured



**Figure 9.** (a) Measured mushy zone thickness along the centre line (blue arrow) shown in (b).

evolution of the columnar mushy zone thickness is plotted with time. The thickness of the columnar zone was measured along the vertical centre line shown in figure 9(b). Obviously, the thickness of the mushy zone grows linearly at first and then the growth saturates. Note that these results are reproducible and thus the second experiment with a similar superheat gives the same result.

The solidification started at different times after the cooling was switched on namely 12 min for the experiments starting at 42 °C and 20 min for the ones starting at 57 °C (see table 1). Because the starting temperatures were different, the time where solidification started was different (section 3.2). Initially, the growth of the columnar mushy zone was linear in time with a slope independent of superheat. In this linear growth regime the dendrite tip velocity is obviously constant. The linear regime lasts between 35 min for the smallest superheat and 40 min for the largest superheat. After one hour, the bottom wall thickness for all experiments reached a plateau at around 25 mm.

The linear growth of the dendrite tip is related to the concentration difference between the bulk concentration and the equilibrium concentration at the dendrite tip. For the first few minutes the bulk concentration does not change as the solidification does not reject enough water-enriched liquid into the bulk. The temperature difference is constant and the growth as well. After 35 to 40 min the evolution of the columnar mushy zone enters a saturated growth.

Another way to quantify the solidification rate was to calculate the total mushy fraction in the cast cell. With a small in-house code this was done using the images taken during the experiment. The results show again the same trend: linear and saturated. In figure 10 the total solid fraction calculated from different experiments is plotted as function of time.

The first solid appeared between 12 min, for the experiment with the starting temperature of 42 °C and respectively 19 to 20 min, for the experiment with the starting temperature of 57 °C. The time to reach the solidification temperature is different because the starting temperature is different (section 3.2). The interesting phenomenon is that the solidification temperature is not fixed (conforming to the phase diagram), it depends as well on the starting temperature. For the 42 °C starting temperature experiment the solidification occurred at

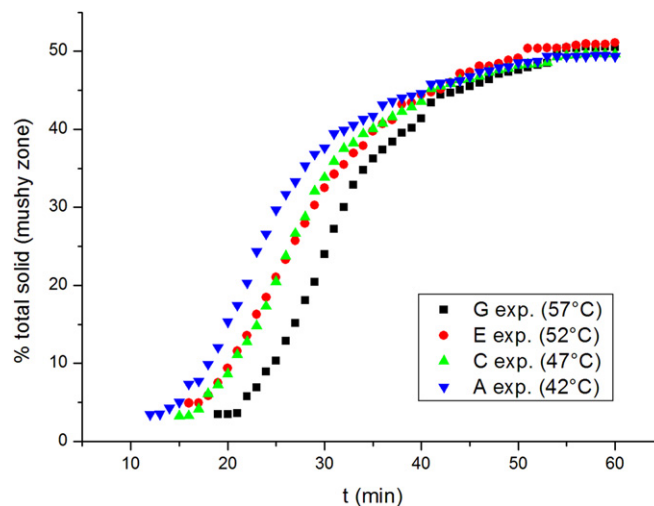


**Figure 10** Total solid fraction calculated from the pictured taken during the solidification experiments.

2746 °C and for the 57 °C starting temperature experiment the solidification temperature is higher 3398 °C. The temperature is measured in the cell's walls. The walls temperature decreases linearly until approximately 6 °C then it is quasi-constant.

At the beginning the growth is linear and the duration of this linear regime is independent of the superheat employed! From the time when the first solid occurred until the end of the linear growth the time is approximately equal for all experiments: 15 to 16 min. Regardless of the different starting temperatures the linear growth always ends around 35% fraction mush in the cell (figure 11). The linear growth stops 3 to 11 min before the wall temperature becomes constant. The total solid fraction, after one hour of cooling, is independent of the starting temperature and always equal to 50% for all cases (figure 11).

#### 4. Conclusions

A solidification experiment with an hypereutectic ammonium chloride-water alloy of 29.57 wt.%  $\text{NH}_4\text{Cl}$  was performed in a rectangular die-cast cell of  $10 \times 10 \times 1 \text{ cm}^3$ . Cooling was uniform for the two walls and the bottom and practically only columnar dendritic growth was observed. The amount of equiaxed crystals was negligible. This is a major difference with the previous observations done under similar experimental conditions (Kharicha *et al* 2013a, 2013b) where intense equiaxed crystals occur and freckle formation was observed. Images were recorded every minute and from the direct visualisation (PIV) and a special image treatment we could extract the thickness of the mushy zone, the total mushy fraction and the flow velocity as function of time.

Different flow regimes were observed and the importance of double-diffusive convection for the flow behaviour was addressed. The results were used to define different flow regimes with the corresponding measured typical velocity pattern. The flow kinetic energy for the entire cell was calculated and the occurrence of a maximum and a subsequent continuous decrease was discussed. For the solidification experiments presented in this paper, the mushy zone developed smoothly and its thickness grew linearly till it followed a saturated law.

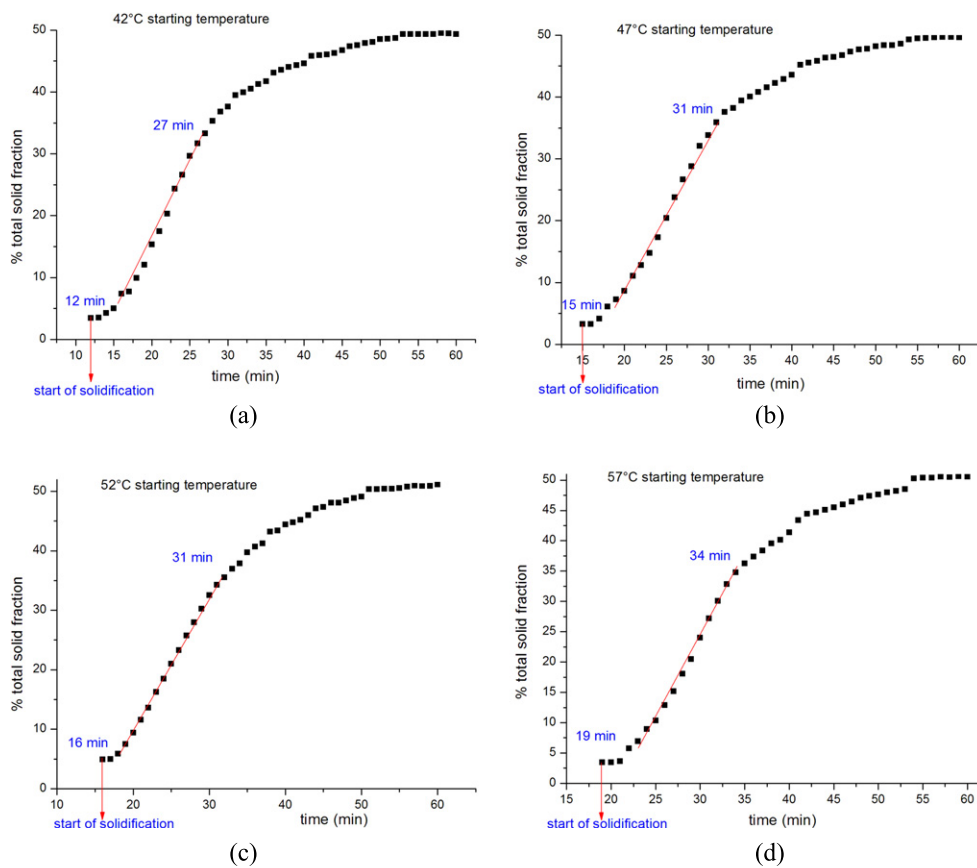


**Figure 11.** Total solid fraction calculated for different experiments with different starting temperatures; (a) 42 °C; (b) 47 °C; (c) 52 °C; (d) 57 °C.

Independent of superheat, the mushy fraction at the end of the linear regime was around 35% and the mushy fraction at the end of the experiment was around 50%.

Note that the primary aim of this descriptive paper is to give an experimental benchmark for the scientific community focusing on the interaction between solidification and hydrodynamics. At present, numerical models are under development worldwide. Therefore, there is an urgent need for experimental data with both flow and solidification measurements in order to validate these numerical models. In future, such validated simulations might shed a light on the parameter which actually controls the bifurcation between purely columnar and mixed columnar equiaxed solidification.

## Acknowledgement

This work was supported by FWF Austrian Science Foundation (P 22614-N22) for which the authors kindly acknowledge.

## References

- Ahmadein M, Wu M, Stefan-Kharicha M, Kharicha A and Ludwig A 2014 A numerical study of the influence of pouring technique on the as-cast structure of Al-Cu ingots *Mater. Sci. Forum* in press
- Beckermann C and Viskanta R 1988 Double-diffusive convection due to melting *Int. J. Heat Mass. Transfer* **31** 2077–89
- Beckermann C and Viskanta R 1989 An experimental study of solidification of binary mixtures with double-diffusive convection in the liquid *Chem. Eng. Comm.* **85** 135–56
- Bejan A 1993 *Heat Transfer* (New York: Wiley)
- Bizon C, Werne J, Predtechensky A A, Julien K, McCormick W D, Swift J B and Swinney H L 1997 Plume dynamics in quasi 2D turbulent convection *Chaos* **7** 107–24
- Chen F 1997 Formation of double-diffusive layers in the directional solidification of binary solution *J. Cryst. Growth* **179** 277–86
- Chen C F and Chen F 1991 Experimental study of directional solidification of aqueous ammonium chloride solution *J. Fluid Mech.* **227** 567–86
- Christenson M S, Bennon W D and Incropera F P 1989 Solidification of an aqueous ammonium chloride solution in a rectangular cavity-II. comparison of predicted and measured results *Int. J. Heat Mass Transf.* **32** 69–79
- Flemings M C 1974 *Solidification Processing* (New York: McGraw-Hill)
- Kharicha A, Stefan-Kharicha M, Wu M and Ludwig A 2012 Exploration of a double diffusive convection during dendritic solidification with a combined volume-averaging and cellular automata model *IOP Conf. Series: Mater. Sci. Eng.* **33** 012115
- Kharicha A, Stefan-Kharicha M, Ludwig A and Wu M 2013a Simultaneous observation of melt flow and motion of equiaxed crystals during solidification using a dual phase particle image velocimetry technique. Part 2: relative velocities *Metall. Mater. Trans. A* **44** 650–60
- Kharicha A, Stefan-Kharicha M, Ludwig A and Wu M 2013b Simultaneous observation of melt flow and motion of equiaxed crystals during solidification using a dual phase particle image velocimetry technique. Part 1: stages characterization of melt flow and equiaxed crystals motion *Metall. Mater. Trans. A* **44** 661–8
- Könözsy L, Eck S, Stefan-Kharicha M, Wu M and Ludwig A 2009 Experimental and numerical investigations of NH<sub>4</sub>Cl solidification in a mould. Part 2: numerical results *Int. J. Cast Metals Res.* **22** 172–4
- Lesoult G, Combeau H and Moukassi M 1993 Interactions between solidification and fluid flow. Effects on cast structures and segregations *J. Phys. IV France* **3** 813–22
- Magirl C S and Incropera F P 1992 Flow and morphological conditions associated with unidirectional solidification of aqueous ammonium chloride *J. Heat Transfer* **115** 1036–43
- Neilson D G and Incropera F P 1991 Unidirectional solidification of a binary alloy and the effects of induced fluid motion *Int. J. Heat Mass Transf.* **34** 1717–32
- Neilson D G and Incropera F P 1993 Effect of rotation on fluid motion and channel formation during unidirectional solidification of binary alloy *Int. J. Heat Mass Transf.* **36** 489–505
- Saffie M G M, Tan F L and Tso C P 2013 A study on the snowing phenomenon in binary alloy solidification *Applied Thermal Engineering* **50** 562–71
- Sample A and Hellawell A 1982 The effect of mold precession on channel and macro-segregation in ammonium chloride- water analog castings *Met. Trans. B* **13** 495–501
- Sample A and Hellawell A 1984 The mechanism of formation and prevention of channel segregation during alloy solidification *Met. Trans. A* **15** 2163–73
- Shih Y-C and Tu S-M 2009 PIV study on the development of double-diffusive convection during the solidification effected by lateral cooling for a super-eutectic binary solution *Appl. Therm. Eng.* **29** 2773–82
- Shih Y-C, Tu S-M and Chiu C-C 2013 Suppressing freckles during solidification due to periodic motion of top liquid layer *Appl. Therm. Eng.* **50** 1055–69
- Solomon T H, Hartley R R and Lee A T 1999 Aggregation and chimney formation during the solidification of ammonium chloride *Phys. Rev. E* **60** 3063–71
- Stefan-Kharicha M, Eck S, Könözsy L, Kharicha A and Ludwig A 2009 Experimental and numerical investigations of NH<sub>4</sub>Cl solidification in a mould. Part 1: experimental results *Int. J. of Cast Metal Res.* **22** 168–71
- Tan F L 2005 An experimental study on channels formation during solidification of aqueous ammonium chloride *Appl. Therm. Eng.* **25** 2169–92

- Wu M, Ludwig A and Fjeld A 2010a Modeling mixed columnar-equiaxed solidification with melt convection and grain sedimentation-part 1: model description *Comp. Mater. Sci.* **50** 32–42
- Wu M, Ludwig A and Fjeld A 2010b Modeling mixed columnar-equiaxed solidification with melt convection and grain sedimentation-part 2: illustrative modeling results and parameter studies *Comp. Mater. Sci.* **50** 43–58